Super-Elastic and Plastic Shock Waves Generated by Lasers

N.A. Inogamov[1,a], V.V. Zhakhovsky[2,3,b], S.I. Ashitkov[3,c], V.A. Khokhlov[1,d], B.J. Demaske[2,e], S.I. Anisimov[1,f], M.B. Agranat[3,g], V.E. Fortov[3,h], and I.I. Oleynik[2,i],

[1] Landau Institute for Theoretical Physics, Russian Academy of Sciences, Chernogolovka, Moscow region, 142432, Russian Federation

[2] Department of Physics, University of South Florida, Tampa, Florida 33620, USA

[3] Joint Institute for High Temperatures, Russian Academy of Sciences, Moscow, 125412, Russian Federation

[a] nailinogamov@gmail.com, [b] vasily@usf.edu, [c] Ashitkov11@yandex.ru, [d] v_a_kh@mail.ru, [e] bdemaske@mail.usf.edu, [f] anisimov@itp.ac.ru, [g] agranat2004@mail.ru, [h] fortov@ihed.ras.ru, [i] oleynik@usf.edu

Keywords: Femtosecond laser-matter interactions, elastic-plastic transformations in laser shocks

Abstract. It is proved that in the femtosecond (fs) laser experiments there is an elastic shock wave (SW), which propagates before the strong plastic shock with plastic pressures of up to few Megabars. We have found that an initial speed of the melting front is larger than a sound speed because of the fast (supersonic) propagation of an electronic thermal wave into metal. It is shown that the steep part of the elastic compression wave separates from the supersonic melting front when the melting front transits from supersonic to subsonic speed of propagation. Later in time this steep part of the elastic compression wave overturns as result of intersections of elastic characteristics and the elastic SW appears. The elastic SW (ElSW) forms from the steep part which corresponds to the intersection of an isochoric line $\rho = \rho_0$ with a melting curve $T_m(p)$. Therefore the elastic pressure $p_{ElSW} \approx p(\rho_0, T_m)$ behind the ElSW is independent from the value of absorbed laser energy F_{abs} and the value of plastic pressure, while the latter is proportional to fluence F_{abs}; here $p(\rho, T)$ is one-temperature equation of state. This remarkable property may be used for experimental definition of melting curve $T_m(p)$.

The thermal wave transfers heat into bulk from the skin-layer of metal, where laser energy was absorbed. The thermal wave propagates fast at an early stage when electrons are much hotter than ions: $T_e >> T_i$. In the case of aluminum - this is the first 2-3 ps after the fs heating laser pulse.

By hydrodynamics and atomistic simulations and comparison of results of modeling with fs experiments, it is found that there is a continuation of an elastic shock Hugoniot to the pressures, which are much higher (10-50 times) than the usually accepted values for the Hugoniot elastic limit.

We have shown that fs lasers are very efficient generators of shocks in condensed matter. We have calculated the elastic and plastic branches of the Hugoniot curves and the spall strength for shocks created by such generators.

A new structure of elastic-plastic SW in metals has been discovered [Zhakhovsky et al., PRL, **107**, 135502 (2011)]. It is a stationary single structure of elastic and plastic shocks, where radiation of strong elastic pressure pulses from the plastic shock front supports the elastic shock front on the fixed distance from the plastic SW. This means that plastic shock front pushes away the elastic wave, instead of overrun it. Prior to that, people thought that the generated together elastic and plastic shock waves can *only* propagate in non-stationary split wave regime, where the plastic wave lags behind the elastic wave with time.

We have studied the fs laser ablation of aluminum, gold, and nickel films. Formation and reflection of pressure and tensile waves, melting, bubble nucleation and cavitation in the molten layer have been studied. It is shown that ablation of molten metal is caused by cavitation and foaming of melt both taking place within the frontal layer of the film irradiated by a laser pulse. We have analyzed the process of freezing of the cavitation bubbles within the surface layer of the metal films. Spall phenomena caused by reflection of a shock wave are investigated on the rear side of the film.

Authors (NAI, SIA, VAK, and MBA) acknowledge support from RFBR grant No. 10-02-00434-a.

1. Super-elastic trace of supersonic melting and laser elastic-plastic shocks

Shocks propagating through crystals may have an elastic component and therefore they differ qualitatively from shocks in liquids and gases because the last are purely plastic. It was shown [1-4] that femtosecond (fs) lasers produce an elastic precursor ahead a very strong plastic shock. This has been proved for aluminum and nickel and for plastic pressures up to a few Megabars. We show here that there are *three* reasons listed below for this surprising behavior (it is unexpected/surprising that an elastic wave survives at so high pressures). Namely, there is supersonic propagation of a two-temperature electron heat conduction wave, *first* [5-7]. This is shown in Fig. 1 (a).

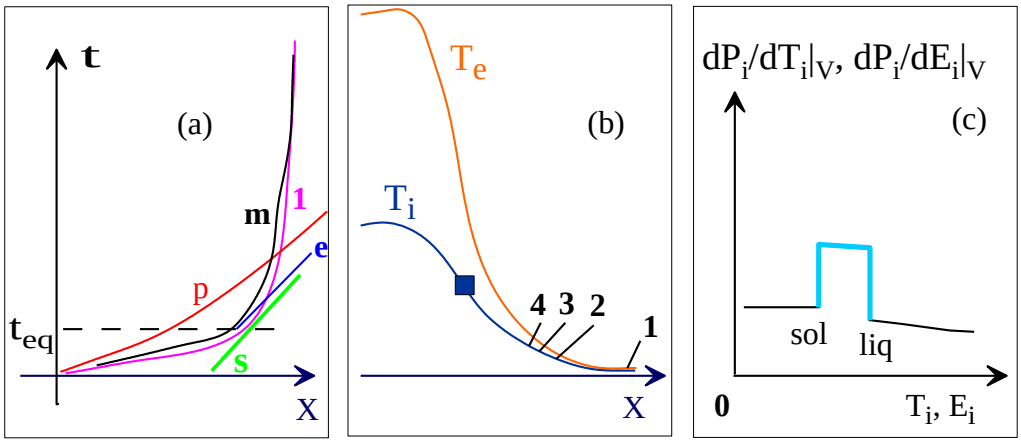

Fig. 1. Formation of separated elastic “e” and plastic “p” compression waves in transonic neck during transition from supersonic to subsonic regime of electron heat penetration. In the transonic neck the trajectory “1” is approximately tangential to the sonic straight line “s”. Prior to the neck the trajectory “1” is steeper than the straight line “s” because this is the supersonic part of the trajectory “1”. (a) The trajectory “1” describes penetration of point where ion temperature is equal to triple point temperature; “m” is a melting zone, solid is at the right side respective to this zone. The melting zone follows the trajectory “1”. Two-temperature [8, 9] relaxation lasts up to $t = t_{eq}$. (b) Electron and ion temperature profiles at the two-temperature stage $t < t_{eq}$. The blue square marks current position of temperature inflection point. Compression wave overturns and forms plastic

shock near this point. The trajectory of the inflection point and the trajectory of plastic shock are shown as the curve "p" in left panel. (c) Changes in the effective Gruneisen parameter during isochoric fs laser heating [5-7]; "sol" and "liq" are solidus and liquidus. They correspond to borders of equilibrium melting.

Second, there is a deviation of a slope of the isochoric pressure dependences $p_i(\rho=\rho_0,T_i)$ and $p_i(\rho=\rho_0,E_i)$ on temperature T_i and internal energy E_i when the isochoric line $\rho=\rho_0$ crosses the two-phase (solid-liquid) mixture zone at the thermodynamic (ρ,T_i) or (ρ,E_i) planes. We neglect influence of T_e on melting in this explanation; for some metals this influence is rather significant. Total pressure is approximately equal to sum of electron and ion pressures $p=p_e+p_i$ [9]; in the approximation used for our hydrodynamic simulations the dependence $p_i(\rho,T_i)$ is taken from one-temperature $T_e=T_i$ equation of state [9]. The two kinks at the instant $t=t_{fix}$ at the spatial pressure profile $p(x,t_{fix})$ are described below. These kinks are connected with solidus and liquidus borders of melting. Fast melting and kinks define process of elastic shock formation. Electron contribution to pressure p_e is smooth function of density and electron temperature. At the supersonic stage of heat propagation the density remains unchanged $\rho=\rho_0$ because sound does not have time to decrease a pressure load. This is an isochoric heating. Therefore density in the function $p_e(\rho,T_e)$ is constant, while temperature $T_e(x,t_{fix})$ is smooth function on depth x. In these conditions pressure p_e does not compensate formation of the kinks. Our two-temperature hydrodynamic simulation confirms appearance of kinks. This simulation includes electron thermal and pressure effects. The borders of the mixture zone from the pure solid and the pure liquid sides are marked as "sol" and "liq" (solidus and liquidus) in Figs. 1 (c) and 2.

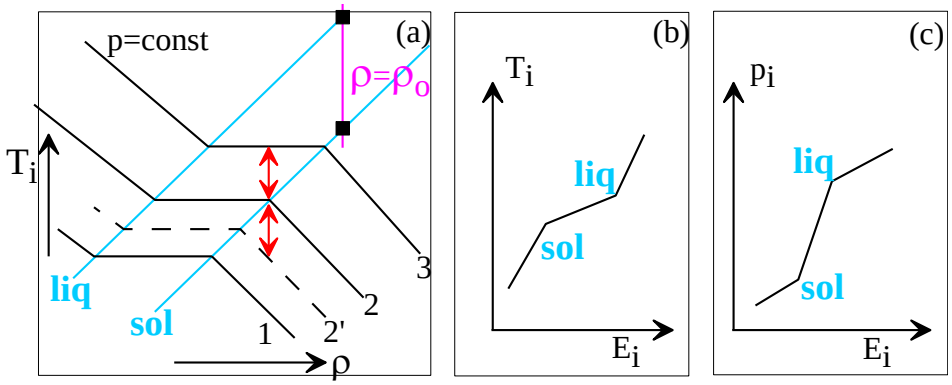

Fig. 2. An explanation how the "hardening" at an isochoric line in a solid-liquid mixture zone appears. This "hardening" is shown also in Fig. 1 (c). Two kinks in Figs. 2 (b) and (c) correspond to two black squares in Fig. 2 (a). In Figs. (b) and (c) the dependencies along an isochoric line $\rho=\rho_0$ are presented.

In Fig. 2 (a) four isobaric curves 1, 2', 2, and 3 are shown. Let us consider a close family of the isobars 1, 2, 3 with infinitesimal pressure shifts between them. The isobars 1, 2, and 3 have an equidistant pressure shift. The upper red arrow in Fig. 2 (a) gives a temperature step between the isobars 2 and 3 inside the melting zone. This zone is limited by the curves solidus "sol" and liquidus "liq". We see that the same temperature step outside the melting zone corresponds to smaller pressure difference – compare the shifts 3-2 and 2-2'. Therefore the derivative

$$\frac{\partial p_i(\rho,T_i)}{\partial T_i}|_V$$

is larger in the melting zone as it is shown in Fig. 1 (c).

Effective heat capacity at constant volume is larger inside the melting zone due to latent heat of melting, see Fig. 2 (b). Nevertheless the increase of the derivative $\frac{\partial p_i(\rho,T_i)}{\partial T_i}|_V$ overcomes the decrease of the derivative $\frac{\partial T_i}{\partial E_i}|_V$ in the melting zone. Therefore the derivative

$$\frac{\partial p_i(\rho,E_i)}{\partial E_i}|_V = \frac{\partial p_i}{\partial T_i}|_V \frac{\partial T_i}{\partial E_i}|_V$$

also is larger in the melting zone as it is shown in Figs. 1 (c) and 2 (c).

Third, the electron heat conduction wave is supersonic only at the two-temperature stage (see, e.g., papers [8, 9] about this stage where electrons are hot: $T_e >> T_i$). This is the third point in the list of the three points explaining why in fs laser experiments the elastic shock forms and survives ahead a very strong plastic shock. Let us emphasize that Mach number of electron heat conduction wave is higher if the ratio t_{eq}/t_s is smaller; here t_{eq} is duration of two-temperature stage, $t_s = d_T/c_s$ is acoustic time scale, d_T is a heat penetration depth. Supersonic penetration is possible at an early stage because Fermi velocity of electrons is much larger than sound velocity c_s [5-7]. The conduction wave transits to subsonic regime of propagation at the end of two-temperature relaxation when electron and ion temperatures T_e and T_i equalizes. During this transition acoustic wave separates from thermal wave because the acoustic wave cannot move slower than velocity of sound c_s. It may be said that supersonic thermal wave emits or radiates sound wave when the thermal wave decelerates down from supersonic to subsonic velocities.

High pressures ~Megabars and plastic shock appear when absorbed fluence F_{abs} J/cm^2 is high enough – order of magnitude higher than an ablation threshold on absorbed energy $F_{abs}|_{abl} \sim 0.1$ J/cm^2. In metals an ablation threshold is typically few times higher than a melting threshold F_m. Therefore at large fluencies the trajectory "1" in Fig. 1 is followed by the melting zone. In these conditions propagation of melting from an irradiated surface into bulk is supersonic at the two-temperature stage while $t < t_{eq}$. Indeed, ion temperature inside the region covered by thermal wave quickly increases above the spinodal curve for melting $T_i > (1.1-1.4)T_m(p)$ (at $t \sim t_{eq}$ hot $T >> T_m$ melt is formed inside this region). Metal in this region melts at atomic time scale ~0.1-1 ps. This is the process of homogeneous, bulk, or volume melting when molten nuclei appear inside whole volume. Melting front expands with supersonic velocity at the stage of volume melting but this is formal or phase velocity of expansion.

In transonic neck, see Fig. 1 (a), volume melting gradually transits to heterogeneous melting. Gradually melting zone between solids and liquidus becomes narrower than thickness of a molten layer behind the melting zone. In Fig. 1 (a) the molten layer remained on the left side relative to the melting zone propagating to the right side. Only trajectory of the solidus (the right border of the melting zone) is shown in Fig. 1 (a) as the trajectory "m". Liquidus is the left border of the melting

zone. It is not shown in Fig. 1 (a) to avoid complication of the Figure. The trajectory "1" runs ahead relative to the trajectory "m" because the trajectory "1" corresponds to melting temperature at low pressures (this is the triple point temperature) while there are elevated temperatures at the trajectory "m" corresponding to melting at elevated pressures, see Fig. 2 (a) and two black squares in this figure. Pressures p_{sol} and p_{liq} in these two squares are rather high; ≈ 4.5 and 11 GPa for aluminum [5-7].

Picture with two clearly seen kinks corresponding to solidus and liquidus has been obtained in hydrodynamic simulation using the thermodynamically equilibrium equation of state. In equilibrium solid begins to melt as melting temperature is achieved. In real situation there are overheated crystals and kinetics of melting. Our molecular dynamics (MD) simulations probe influence of these kinetic effects onto a hydrodynamic picture. It has been found that all main features, concerning supersonic isochoric melting and isochoric "hardening" shown in Figs. 1 (c) and 2, remains. Namely these features are related to generation of spatially separated plastic and elastic shocks. But there is one difference also. In MD the kink corresponding to liquidus is pronounced, while the lower on pressure kink corresponding to solidus is smeared.

At large fluencies (ten and more times higher than ablation threshold) maximum pressures and temperatures are much higher than pressures and temperatures in the melting zone between two black squares in Fig. 2 (a), see Fig. 1 (b). Even pressure and temperature in the infection point in Fig. 1 (b) are much higher than the melting values (the digits 3 and 4 in Fig. 1b). The digits 1, 2, 3, and 4 in Fig. 1 (b) correspond to the room temperature, triple point, solidus, and liquidus, respectively. The melting zone 3-4 in Fig. 1 (b) is located at the far right end of the heated layer as result of this difference in temperatures.

Compression wave gets detached (breaks away) from a temperature profile at the final stage of supersonic heat penetration (this is the transonic neck in Fig. 1a). After detaching, the compression wave carries along characteristics the inflection point shown in Fig. 1 (b) and carries the acoustic traces of the melting zone. These traces correspond to the kinks at the borders of a melting zone. These traces of the kinks also propagate along the characteristics running to the right side in Fig. 1 (a). The acoustic propagation of the kink traces begins at the transonic neck. The curve "p" in Fig. 1 (a) gives the trajectory of the inflection point and gives the trajectory of the plastic SW after breaking of plastic wave in the inflection point. The curve "m" in Fig. 1 (a) gives the trajectory of the kink connected with solidus only at the supersonic stage of heat penetration. The acoustic trace of the solidus corresponds to the curve "e" in Fig. 1 (a) at the subsonic stage of heat penetration.

Significant spatial separation of the kinks 3 and 4 from the inflection point in Fig. 1 (b) at the supersonic heat stage keeps for some time the acoustic traces of the kinks from being overrunned by plastic SW (PlSW) when the PlSW appears in the inflection point. As was said above, the kinks appear at the smooth, heat conduction created temperature profile as a result of sharp variation of Gruneisen parameter in a melting zone due to melting, see Fig. 1 (c).

Simulations show that pressure gradient between the kinks is higher than the gradient outside the kinks. This circumstance significantly accelerates breaking of compression wave at the interval between the acoustic traces of the kinks. Consequently, there are two independent wave-breakings. One corresponds to the inflection point belonging to high pressures, while another – to the interval between the traces of the kinks at relatively low pressures between p_{sol} and p_{liq} (4.5 and 11 GPa for Al). Simulations show that in fs experiments metal remains elastic at the pressures

$\sim p_{ElSW} \approx p(\rho_0, T_m)$. These pressures correspond to the traces of the kinks. Therefore the large pressure difference corresponding to the large spatial separation between the two wave-breakings keeps ElSW from disappearing in PlSW.

Simulations also show that the PlSW decelerates and stops *before* it overruns the ElSW. Consequently, ElSW exists all time after its appearance. This conclusion corresponds to our limited range of fluencies $F_{abs} \sim 1$ J/cm^2. Stopping of PlSW produces a plastically modified surface layer. Thickness $l_{plast}(F_{abs})$ of this layer increases with increase of absorbed fluence F_{abs}. This thickness is much less than the thickness predicted by hydrodynamic simulation with usual value of Hugoniot elastic limit (HEL) because in the fs laser experiment conditions the elastic state survives at much higher stresses.

High pressures inside a main compression wave significantly influence melting temperature $T_m(p)$. Melting zone slowly decelerates at the subsonic stage of heat penetration. This may be seen in Fig.1 (a) - the trajectory "m", see also Fig. 3. There is a sub-stage "acc" in Fig. 3 with limited in time a weak acceleration of the melting zone. This acceleration takes place when the main compression wave passes the melting zone and leaves behind the melting zone in the process of acoustic propagation of compression wave to the right side in Figs. 1 (a) and 3. Pressures in the melting zone drop down when the compression wave leaves the melting zone. The decrease of pressure decreases the melting temperature $T_m(p)$ down to triple point temperature T_3 and even below the temperature T_3 if pressures become negative. This decrease accelerates the melting front along a gradient of temperature in the thermal wave because unloaded metal melts at lower temperature. The trajectory "m" in Fig. 1 (a) coincides with trajectory "1" after the drop of temperature at a melting front down to T_3.

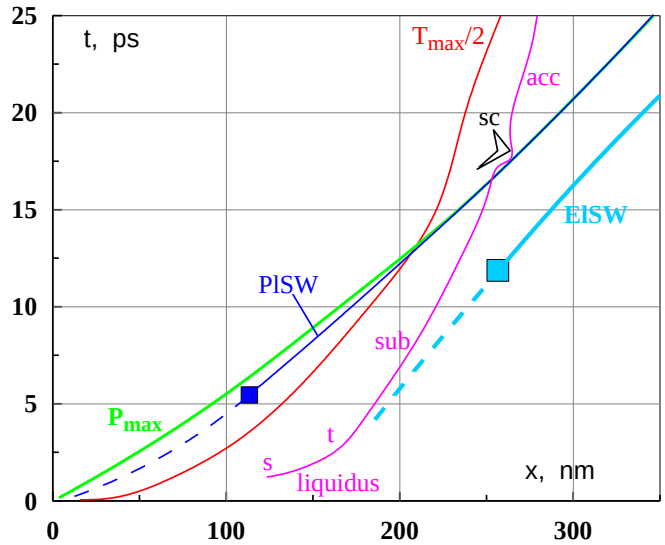

Fig. 3. Transition from supersonic "s" to subsonic "sub" regime, radiation of an elastic shock (ElSW), and passing of main shock (PlSW) through the melting front (here trajectory of liquidus is shown). Propagation of the point "$T_{\max}/2$" with a current value of temperature equal to a half of the instant value of maximum temperature presents process of thermal expansion into target.

The curve " $p_{\max}$" in Fig. 3 gives an instant position of the point with an instant maximum pressure; function $p_{\max}(t)$ decreases with time. The deep blue dashed curve, the deep blue square, and the curve "PlSW" present a trajectory of the inflection point, the point where wave-breaking takes place, and the trajectory of strong (relative to isochoric melting pressures) plastic shock respectively. We see that as a result of subsonic (relative to PlSW) drift of characteristics behind the shock "PlSW", the maximum " $p_{\max}$" begins to coincide with position of PlSW.

Compressed metal remains elastic in Fig. 3 inside the strip between the curve of solidus from the left side (or curve PlSW) and the trajectory ElSW from the right side. The light blue dashed curve in Fig. 3 detached from melting zone at the transonic neck "t" presents an inflection point inside the trajectories of the traces of the kinks. In the point marked by the light blue square the elastic compression wave overturns and forms elastic shock "ElSW".

As we see, there is a rich set of phenomena connected with (a) supersonic propagation of thermal wave and melting front into the bulk of a target at the two-temperature stage, (b) transonic neck, transition to subsonic propagation regime, and (c) radiation of strong acoustic perturbation separating from a melting front at the transonic stage. It is found that (i) this acoustic perturbation evolves into elastic SW, (ii) amplitudes of the elastic perturbation weakly depend on absorbed fluence. (iii) There is the deceleration-acceleration-deceleration episode at the melting front trajectory. It is marked as "acc" Fig. 3. The episode "acc" in Fig.3 is a result of significant dependence of melting temperature on pressure $T_m(p)$ and decrease of pressure at the melting front due to interplay between the tail of the initially supersonic thermal wave from the one side and the strong compression/shock wave passing through molten metal and melting front from the another side. The compression/shock wave begins to outrun thermal wave when the latter transfers to subsonic regime.

(iv) In the (fast heating-melting)/(sound generation) history there is a short episode marked as "sc" (supercooled liquid) in Fig. 3 when increase of melting temperature $T_m(p)$ due to the pressure rise in strong PlSW is larger than local temperature of molten metal ahead the PlSW plus a temperature increase as a result of shock compression. In this case liquid behind the "liquidus" curve in Fig. 3 transfers for a short time into state of supercooled liquid. The episode "sc" is connected with sharp pressure rise after arrival of PlSW. Decrease of pressure in rarefaction wave behind the PlSW decreases temperature $T_m(p)$. Therefore liquid returns back into equilibrium liquid state. PlSW sweeps matter along its propagation.

2. Super-elastic laser SW

Outstanding results concerning elastic-plastic transition and Hugoniot elastic limit (HEL) have been received recently [10-14]. They are based and supported by theoretical predictions [10, 11] were high stress elastic states have been found. This allows clearly understand surprising experimental results [12-14] obtained with fs [12] and subnanosecond [13, 14] laser shock drivers. We clearly see super-elastic shocks in aluminum, nickel, and gold at stresses order of magnitude (!) higher than usually accepted values.

Crystal, uni-axially compressed from force free $(p = 0)$ state, transfers into a metastable state even under an arbitrary small uni-axial stress σ. Decay time τ of this state is a strong function on magnitude σ (τ is very large for small σ), temperature, and weak but significant function on duration time under load (the decay time also depends on dislocation structure prior to stress). In this

sense there are no very definite values for HEL – the stress HEL weakly depends on duration of loading. Papers [10-14] present the upper end values near an absolute strength for the HEL. Different dislocation mechanisms are responsible for elastic-plastic transformation depending on magnitude σ. At the highest magnitudes achieved in laser experiments [10-14] generation of dislocation loops by mechanism of thermal fluctuation dominates. At less high stresses preexisting dislocations become more important.

Relative positions of elastic, plastic, and molten parts of the shock adiabatic curves at the $(V/V_0, p)$ plane (compression–pressure plane) are shown in Fig. 4 (a). Point $(V/V_0 = 1, p = 0)$ in Fig. 4 corresponds to the state ahead the SW. This is force free $(p = 0)$ uncompressed $V = V_0$ state; $V_0 = 1/\rho_0$ is its specific volume. Elastic Hugoniot (1-HEL*) forms a separate branch. The HEL* is an end point of the elastic branch [3, 4, 11, 15]. Now an elastic branch is extended far beyond the usually accepted position of the end point HEL of the elastic shock adiabatic curve. The usual HEL is marked by the arrow in Fig. 4 (a). The point HEL* corresponds to strong compressions $1 - V/V_0 = (0.1 \div 0.15)$, high stresses ($\approx 33$ GPa for Al, ≈ 60 GPa for Ni), and large piston velocities ~1 km/s – compare with usually accepted values for the point HEL: compression ~1%, stress 0.1-1 GPa, and piston velocities ~50 m/s.

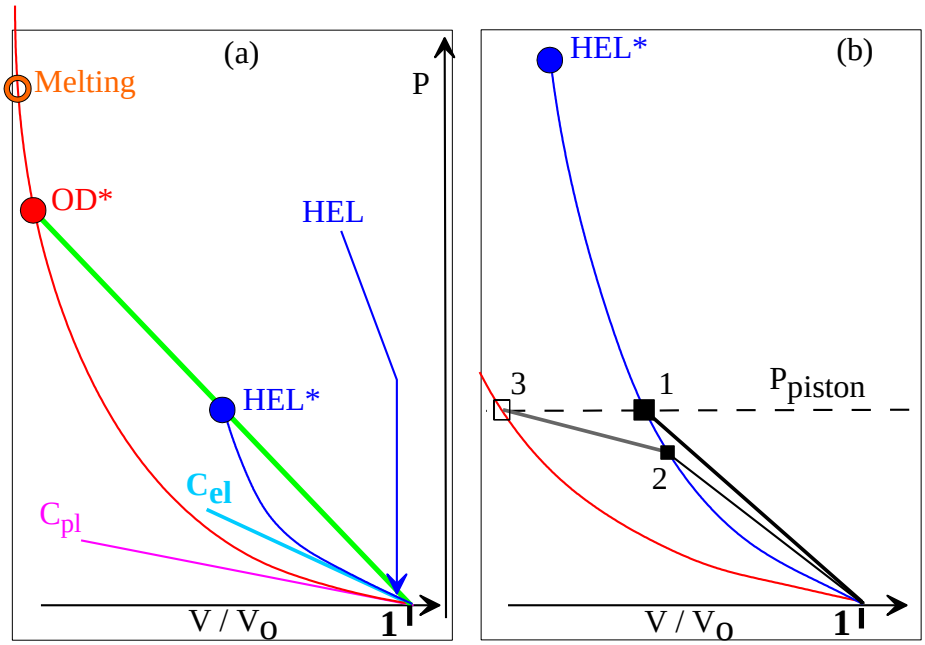

Fig. 4. (a) Elastic (1-HEL*) and plastic (1-OD*-Melting-) branches of Hugoniot adiabatic curves. Here $p = |\sigma|$; HEL is Hugoniot elastic limit; OD* is Over-Driven SW. Above the point OD* the pure plastic SW exists. (b) Evolution of SW created by instantaneous beginning of piston motion. Enlarged view of left panel. We support constant pressure p_{piston} at the piston. The jump 1-1 from $p = 0$ to piston pressure presents purely elastic SW shortly after beginning of motion. After a while, the elastic SW moves away from a piston to a distance d, its amplitude decays from the intersection point 1 to the intersection point 2, and a plastic SW 2-3 appears somewhere near a piston, because the distance d achieves the value $d_{nucl}(|\sigma| = p_2)$ which is enough for creation of viable dislocation loop by thermal fluctuations at the pressure p_2 behind an elastic SW corresponding to the point 2 in Fig. 4 (b).

Fig. 4 (b) illustrates how a SW evolves after its sudden creation. Fig. 4 (b) explains why at the relatively low absorbed fs laser fluencies $\sim(F_m \div F_{abl})$ and pressures ~10 GPa the fs laser shock remains *purely* elastic while at the higher fluencies, the order of magnitude or more higher than an ablation threshold F_{abl}, the split elastic-plastic SWs appear; here F_m is a melting threshold. Indeed, the thickness of the fs laser SW is weakly depended on fluence and is finite ~100 nm. Therefore pressures above some limited value are necessary to decrease the function $d_{nucl}(\sigma)$ down to the thickness of the laser SW. As was written under Fig. 4, the function $d_{nucl}(\sigma)$ defines time $\sim d_{nucl}/c_s$ for creation of viable dislocation loop by thermal fluctuations at the longitudinal stress σ behind an elastic SW.

3. Single wave elastic-plastic structures

A new regime of elastic-plastic waves in metals has been discovered recently [15, 16]. This is a steady-state single wave structure of elastic and plastic shocks: 1W2Z – single wave (1W) and two (elastic and plastic) zones (2Z). Radiation of strong elastic pressure pulses from the plastic shock front supports the elastic shock front on the fixed distance from the plastic SW. This means that PlSW pushes away the ElSW, instead of overrun it. Previously only non-stationary split wave regime 2W2Z (two waves with different propagation velocities and two zones) was known. It corresponds to two jumps 1-2-3 shown as two Rayleigh lines in Fig. 4 (b).

Authors (NAI, SIAsh, VAK, SIAn, MBA) acknowledge support from RFBR grant No. 10-02-00434-a

References

[1] N.A. Inogamov, V.V. Zhakhovsky et al.: JETP Lett. Vol. 93(4) (2011), p. 226

[2] N.A. Inogamov, V.A. Khokhlov, Yu.V. Petrov, S.I. Anisimov, V.V. Zhakhovsky, B.J. Demaske, I.I. Oleynik, C.T. White, S.I. Ashitkov, K.V. Khishchenko, M.B. Agranat, V.E. Fortov: *Ultrashort elastic and plastic shock waves in aluminum*, Eds. Tracy Vogler and Mark Elert. AIP Conf. Proc. Shock Compression of Condensed Matter – 2011. AIP Conf. Proc. Vol. 1426, pp. 909-912 (2012); doi: 10.1063/1.3686425

[3] B.J. Demaske, V.V. Zhakhovsky, N.A. Inogamov, C.T. White , I.I. Oleynik: *MD simulations of laser-induced ultrashort shock waves in nickel*, ibid pp. 1163-1166 (2012); doi: 10.1063/1.3686486

[4] B.J. Demaske, V.V. Zhakhovsky, N.A. Inogamov, C.T. White, I.I. Oleynik: *Evolution of metastable elastic shock waves in nickel*, ibid pp. 1303-1306 (2012); doi: 10.1063/1.3686520

[5] N.A. Inogamov, S.I. Ashitkov, V.V. Zhakhovsky, V.V. Shepelev, V.A. Khokhlov, P.S. Komarov, M.B. Agranat, S.I. Anisimov, V.E. Fortov: Appl. Phys. A Vol. 101(1) (2010), p. 1

[6] N.A. Inogamov, V.V. Zhakhovskii, S.I. Ashitkov, V.A. Khokhlov, V.V. Shepelev, P.S. Komarov, A.V. Ovchinnikov, D.S. Sitnikov, Yu.V. Petrov, M.B. Agranat, S.I. Anisimov, V.E. Fortov: *Laser acoustic probing of two-temperature zone created by femtosecond pulse*, Contrib. Plasma Phys., v. 51, No. 4, 367 – 374 (2011)

[7] N.A. Inogamov, V.V. Zhakhovsky, S.I. Ashitkov, M.B. Agranat, P.S. Komarov, V.A. Khokhlov, V.V. Shepelev: *Pump-probe method for measurement of thickness of molten layer produced by ultrashort laser pulse*, AIP Conf. Proc. Vol. 1278 (2010), p. 590; doi: 10.1063/1.3507151

[8] N.A. Inogamov, Yu.V. Petrov: JETP Vol. 110(3), (2010), 446

[9] N.A. Inogamov, Yu.V. Petrov, V.A. Khokhlov et al.: Santa-Fe, High Power Laser Ablation (HPLA-2012) Proc. (accepted). To be published as AIP Conf. Proc.
[10] M.B. Agranat, S.I. Anisimov, S.I. Ashitkov et al.: JETP Lett. Vol. 91 (9) (2010), p. 471
[11] V.V. Zhakhovskii, N.A. Inogamov: JETP Lett., Vol. 92(8) (2010), p. 521
[12] S. I. Ashitkov, M. B. Agranat, G. I. Kanel' et al.: JETP Lett. Vol. 92 (2010), p. 516
[13] V.H. Whitley, S.D. McGrane et al.: J. Appl. Phys. Vol. 109 (2011), 013505
[14] J.C. Crowhurst, M.R. Armstrong, K.B. Knight et al.: Phys. Rev. Lett. Vol. 107 (2011), 144302
[15] V.V. Zhakhovsky, M.M. Budzevich et al.: Phys. Rev. Lett. Vol. 107 (2011), 135502
[16] V.V. Zhakhovsky, M.M. Budzevich, N.A. Inogamov, C.T. White, I.I. Oleynik, *Single two-zone elastic-plastic shock waves in solids*, Eds. Tracy Vogler and Mark Elert. AIP Conf. Proc. Shock Compression of Condensed Matter – 2011. AIP Conf. Proc. Vol. 1426, pp. 1227-1232 (2012); doi: 10.1063/1.3686502